JACS
JOURNAL OF THE AMERICAN CHEMICAL SOCIETY
Article
pubs.acs.org/JACS

Redox Active Ion-Paired Excited States Undergo Dynamic Electron Transfer

Ludovic Troian-Gautier, Evan E. Beauvilliers, Wesley B. Swords, and Gerald J. Meyer*

Department of Chemistry, University of North Carolina at Chapel Hill, Chapel Hill, North Carolina 27599-3290, United States

Supporting Information

ABSTRACT: Ion-pair interactions between a cationic ruthenium complex, $[Ru(dtb)_2(dea)][PF_6]_2$, $\mathbf{C1}^{2+}$ where **dea** is 4,4′-diethanolamide-2,2′-bipyridine and **dtb** is 4,4′-di-*tert*-butyl-2,2′-bipyridine, and chloride, bromide, and iodide are reported. A remarkable result is that a 1:1 iodide:excited-state ion-pair, $[\mathbf{C1}^{2+}, \mathbf{I}^-]^{+*}$, underwent diffusional electron-transfer oxidation of iodide that did not occur when ion-pairing was absent. The ion-pair equilibrium constants ranged 10^4–10^6 M^{-1} in CH_3CN and decreased in the order $Cl^- > Br^- > I^-$. The ion-pairs had longer-lived excited states, were brighter emitters, and stored more free energy than did the non-ion-paired states. The ^1H NMR spectra revealed that the halides formed tight ion-pairs with the amide and alcohol groups of the **dea** ligand. Electron-transfer reactivity of the ion-paired excited state was not simply due to it being a stronger photooxidant than the non-ion-paired excited state. Instead, work term, ΔG_w was the predominant contributor to the driving force for the reaction. Natural bond order calculations provided natural atomic charges that enabled quantification of ΔG_w for all the atoms in $\mathbf{C1}^{2+}$ and $[\mathbf{C1}^{2+}, \mathbf{I}^-]^{+*}$ presented herein as contour diagrams that show the most favorable electrostatic positions for halide interactions. The results were most consistent with a model wherein the non-ion-paired $\mathbf{C1}^{2+*}$ excited state traps the halide and prevents its oxidation, but allows for dynamic oxidation of a second iodide ion.

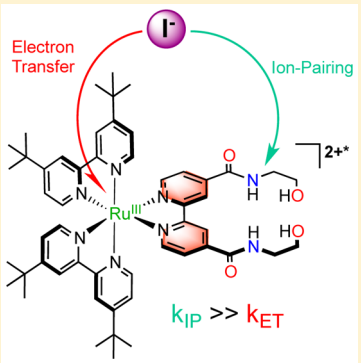

INTRODUCTION

Excited-state electron-transfer reactions are of general importance as they provide a means to convert solar energy into stored potential energy in the form of redox equivalents. Bimolecular reactions generally occur by two mechanisms.[1] The first has been termed *dynamic* electron transfer wherein the excited state diffuses to a redox active species before electron transfer occurs. In an alternative *static* mechanism, a ground-state adduct between the chromophore and the redox active species gives rise to a nonemissive species that undergoes light-driven electron transfer without a diffusional step. Ground-state adduct formation is often enhanced by Coulombic attraction and ion-pair formation. This manuscript reports the first example of an ion-pair that undergoes diffusional excited-state electron transfer that does not occur in the absence of ion-pairing.

Ion-pairs are comprised of oppositely charged ions that share all or part of their solvation shell and possess a binding energy greater than the thermal energy. It is generally accepted that ion-pairs are able to adopt a variety of structures in fluid solution.[2−5] For example, a *contact ion-pair* (sometimes called a tight or intimate ion-pair) is formed when no solvent molecules are located between the ions, like that reported here, Scheme 1. Likewise, a *solvent separated ion-pair* is formed when solvent molecules exist between the ions that decrease the donor–acceptor electronic coupling for redox active ion-pairs.

It has also been recognized that ion-pairing can be enhanced by the presence of functional groups that form specific adducts with the ions. The halide receptor on the **dea** ligand of $\mathbf{C1}^{2+}$ utilizes hydrogen bonding alcohol and amide functional groups that have been previously used to recognize halide ions.[6−11] Visible spectroscopy and ^1H NMR data reported herein demonstrate that chloride, bromide, and iodide all form strong 1:1 adducts with this ruthenium complex that are well formulated as contact ion-pairs. The equilibrium in dichloromethane fell so far to the right that the precise values could not be determined while equilibrium constants in the range of $K_{ip} = 10^4$–10^6 M^{-1} were measured in more polar acetonitrile solutions. Interestingly, these adducts had longer-lived excited states and stored more free energy in their excited states than did the non-ion-paired complex. Furthermore, there was no evidence of static electron-transfer reactivity in the 1:1 ion-pairs. Instead, the ion-pair underwent efficient dynamic iodide photooxidation that did not occur in the absence of the ion-pair. To our knowledge, this represents the first example of diffusional excited-state electron transfer enabled by ion-pair formation between redox active donors and acceptors. The relevance of these findings to emerging classes of "third generation" solar cells that utilize iodide is discussed.

RESULTS

The synthesis of complex $\mathbf{C1}^{2+}$, $[Ru(dtb)_2(dea)][PF_6]_2$ where **dea** is 4,4′-diethanolamide-2,2′-bipyridine and **dtb** is 4,4′-di-

Received: October 31, 2016
Published: December 2, 2016

DOI: 10.1021/jacs.6b11337
J. Am. Chem. Soc. 2016, 138, 16815–16826

Scheme 1. Proposed Ion-Pairing Equilibrium between $C1^{2+}$ and Halide Ions

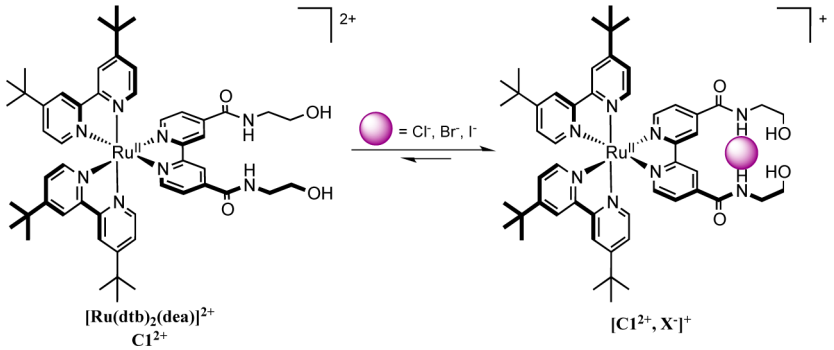

Scheme 2. Synthesis of Complex $C1^{2+}$

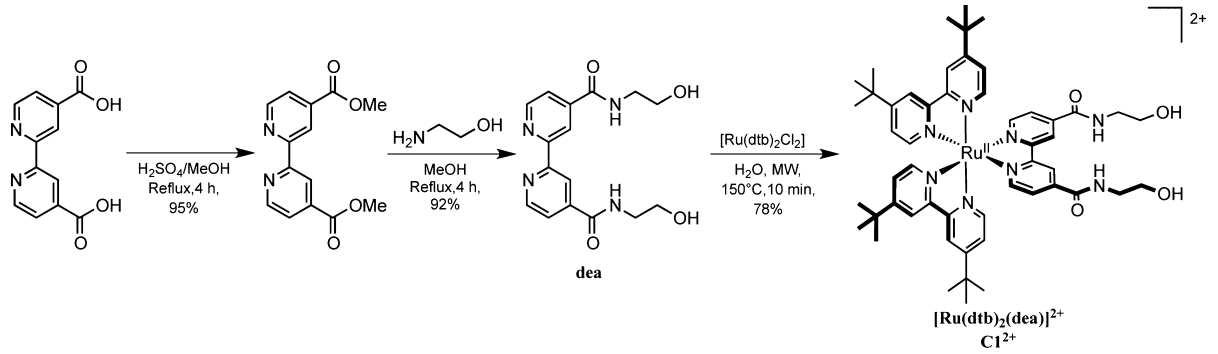

tert-butyl-2,2′-bipyridine, is presented in Scheme 2. The 2,2′-bipyridine-4,4′-dicarboxylic acid was esterified by a modified literature procedure with a 95% yield.[12] Substitution of 4,4′-dimethylester-2,2′-bipyridine by ethanolamine was achieved in methanol to yield the desired **dea** ligand in a 92% yield. Coordination to ruthenium was achieved under microwave irradiation in water and afforded $C1^{2+}$ with a 78% yield.

The photophysical properties of complex $C1^{2+}$ were studied in both acetonitrile (CH_3CN) and dichloromethane (CH_2Cl_2). The steady-state UV–vis absorption spectrum in neat CH_2Cl_2, shown in Figure 1, displayed the characteristic ground-state absorption features of ruthenium polypyridyl complexes. The low energy absorption between 420 and 500 nm were attributed to typical metal-to-ligand charge-transfer (MLCT) transitions (eq 1), whereas the higher energy absorbance was attributed to ligand centered (LC) $\pi \rightarrow \pi^*$ transitions.

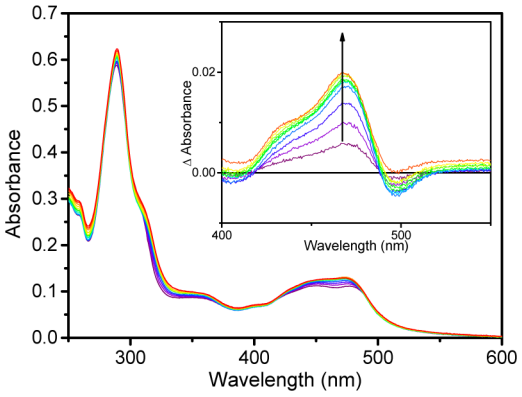

Figure 1. Absorption changes of $C1^{2+}$ upon titration of chloride from 0 to 15 equiv in CH_2Cl_2. Inset shows the difference between the absorption spectrum after each addition of chloride and the initial spectrum. Arrow indicates the direction of change in the spectra with increasing chloride concentration.

$$[Ru^{II}(dtb)_2(dea)]^{2+} + h\upsilon \rightarrow [Ru^{III}(dtb)_2(dea^-)]^{2+*} \quad (1)$$

Light excitation of $C1^{2+}$ resulted in photoluminescence (PL) with a maximum at 670 nm that could be observed by the unaided eye. Time-resolved PL decays generated with pulsed laser excitation of $C1^{2+}$ were well described by a first-order kinetic model, from which excited-state lifetimes were abstracted, 745 ns and 1.32 μs in CH_3CN and CH_2Cl_2 respectively. The photophysical properties of $C1^{2+}$ in neat solution and with added halides are reported in Table 1. Addition of the tetrabutylammonium (TBA^+) salts of chloride, bromide, or iodide to CH_3CN solutions of $C1^{2+}$ resulted in measurable changes in the steady-state absorbance spectra. These absorbance changes are shown in Figure 1 for chloride addition to a solution of $C1^{2+}$ in CH_2Cl_2. Ion-pair equilibrium constants (K_{ip}) abstracted from a modified Benesi–Hildebrand analysis were greater than 10^6 M^{-1} for all the halides in CH_2Cl_2, but were about 2 orders of magnitude smaller in CH_3CN decreasing in the order $Cl^- > Br^- > I^-$.[13,14]

Chloride and iodide ^1H NMR titrations were performed in CD_3CN and CD_2Cl_2 with representative data given in Figure 2. Significant downfield shifts of the amide protons, the protons on the bipyridine 3,3′ carbons, and the hydroxyl protons of the **dea** ligand were observed. Interestingly, in CD_2Cl_2, the hydroxyl protons were shifted the furthest (Δppm of 1.96) with the addition of chloride and the least for iodide (Δppm of 0.52), Figures S13–S21. Protons on the **dtb** ligands were not appreciably affected by the halide additions. The ion-pairing equilibrium stoichiometry was determined by the method of

DOI: 10.1021/jacs.6b11337
J. Am. Chem. Soc. 2016, 138, 16815–16826

Table 1. Equilibrium Constants and Photophysical Properties of $C1^{2+}$ and $[C1^{2+}, X^-]^+$

solvent	species	$K_{ip,GS}$ (M^{-1})	$K_{ip,ES}$ (M^{-1})	λ_{max} PL (nm)	τ (ns)	Φ_{PL}	k_r ($\times 10^4$ s^{-1})	k_{nr} ($\times 10^6$ s^{-1})
CH_3CN	$C1^{2+}$	–	–	685	745	0.044	6.0	1.32
	$+Cl^-$	85×10^4	$>10^6$[a]	675	960[b]	0.063[b]	6.5[b]	0.97[b]
	$+Br^-$	9.0×10^4	5.5×10^4	678	945[b]	0.058[b]	6.2[b]	0.99[b]
	$+I^-$	1.7×10^4	0.6×10^4	681	820[b]	0.051[b]	6.2[b]	1.16[b]
CH_2Cl_2	$C1^{2+}$	–	–	670	1320	0.083	6.3	0.70
	$+Cl^-$	$>10^6$[a]	$>10^6$[a]	645	1830[b]	0.165[b]	9.0[b]	0.46[b]
	$+Br^-$	$>10^6$[a]	[c]	647	1790[b]	0.122[b]	6.8[b]	0.49[b]
	$+I^-$	$>10^6$[a]	[c]	650	1550[b]	0.095[b]	6.1[b]	0.58[b]

[a]Equilibrium constant was too large to be measured; therefore, a minimum is given. [b]Measured after the addition of 1 equiv of the halide. [c]Could not be measured due to quenching induced by halide addition.

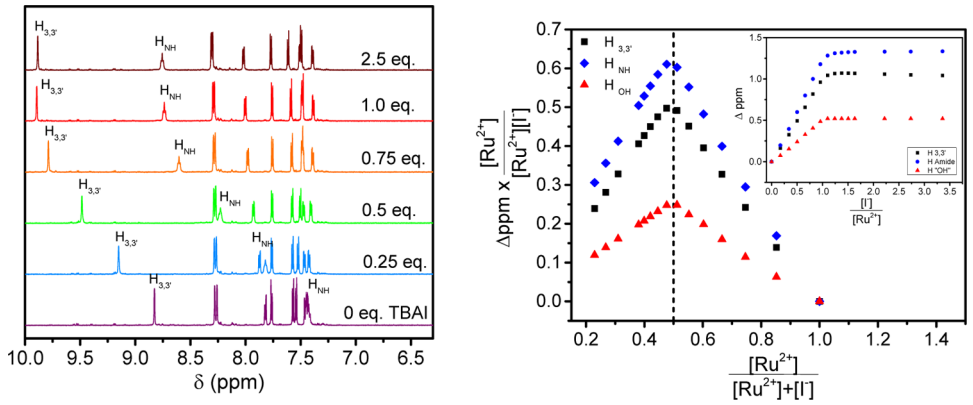

Figure 2. ^1H NMR titration of $C1^{2+}$ with tetrabutylammonium iodide in CD_2Cl_2 (left). Job plot analysis for the NMR titration data (right). Inset represents the observed change in chemical shift of selected protons upon addition of iodide.

continuous variation through a Job plot[15] that revealed a 1:1 Ru:X^- ratio (Figure 2).

The addition of 1 equiv of Cl^-, Br^-, or I^- to a CH_2Cl_2 solution of $C1^{2+}$ resulted in an increase of the PL intensity concomitant with a blue shift in the peak maximum that followed the trend $Cl^- > Br^- > I^-$. The magnitude of this shift was between 25 and 20 nm, which corresponded to ~60 meV. The excited-state lifetime also increased from 1.32 to 1.83, 1.79, and 1.55 μs upon the addition of 1 equiv of Cl^-, Br^-, and I^-, respectively. Representative steady-state PL data for the addition of iodide in CH_2Cl_2 are shown in Figure 3. A less intense increase and blue shift were also observed in CH_3CN that followed the same halide trend.

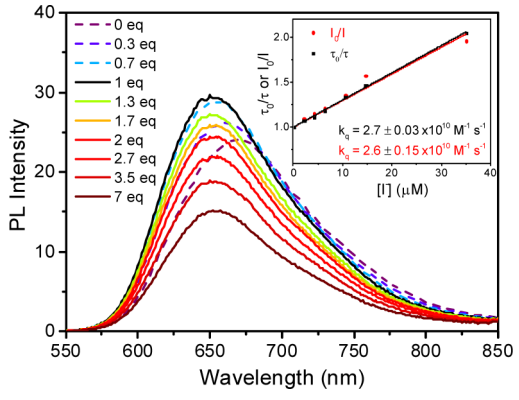

Figure 3. Steady-state PL titration of TBAI into a 10 μM $C1^{2+}$ solution in CH_2Cl_2. Inset shows the Stern–Volmer plot starting after 1 equiv of iodide (solid spectra).

The PL spectral changes saturated at a high halide concentrations in CH_3CN and for chloride in CH_2Cl_2 that enabled the excited-state ion-pairing equilibrium constants, $K_{ip,ES}$, to be abstracted, Table 1. The absorbance and PL maximum of the ion-paired species are reported in Table 1 with the abstracted ion-pairing constants. The UV–vis and PL spectra of the ion-pairs are shown in Figures S6–S12. With the exception of chloride, when the solution ionic strength was increased by the addition of 100 mM $TBAClO_4$, the absorbance and PL spectral shifts associated with iodide ion-pairing and excited-state quenching were lost, Figure S22–S25.

The addition of iodide or bromide beyond 1 equiv led to excited-state quenching in CH_2Cl_2. Stern–Volmer analysis of the steady-state (I) or the time-resolved PL data (τ) yielded a Stern–Volmer constant, K_{SV}, of 4.0×10^5 M^{-1}, eqs 2 and 3. This provided a quenching rate constant, $k_q = 2.6 \pm 0.1 \times 10^{10}$ M^{-1} s^{-1}, eq 3, indicating that only dynamic quenching was operative. It should be noted that there was no evidence of ligand loss photochemistry over the course of the experiments and no evidence of excited-state electron transfer in CH_3CN. The equilibrium constant for iodide and bromide with $C1^{2+}$ could not be accurately determined by PL measurements in CH_2Cl_2 due to the observed quenching.

$$I_0/I = 1 + K_{SV}[X^-] \quad (2)$$

$$\tau_0/\tau = 1 + K_{SV}[X^-] \quad (3)$$

$$k_q = K_{SV}/\tau_0 \quad (4)$$

Transient absorption spectroscopy was performed in CH_2Cl_2 solutions of $C1^{2+}$, Figure 4. The transient absorption spectrum of $C1^{2+}$ in neat CH_2Cl_2 following 532 nm pulsed laser

DOI: 10.1021/jacs.6b11337
J. Am. Chem. Soc. 2016, 138, 16815–16826

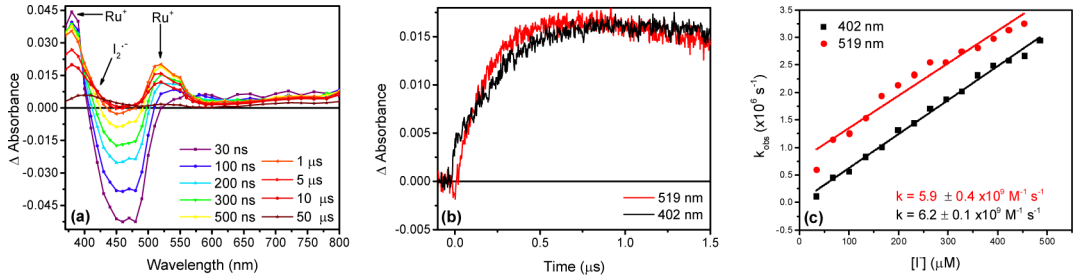

Figure 4. Transient absorption spectrum of $\mathbf{C1}^{2+}$ in CH_2Cl_2 with 20 equiv of iodide (a), single wavelength transient absorption traces at 402 and 519 nm (b), and observed rate at these wavelengths at various concentrations of iodide overlaid with linear fits (c). All experiments were performed at a $\mathbf{C1}^{2+}$ concentration of 70 μM in CH_2Cl_2 with a laser fluence of 3 mJ/pulse.

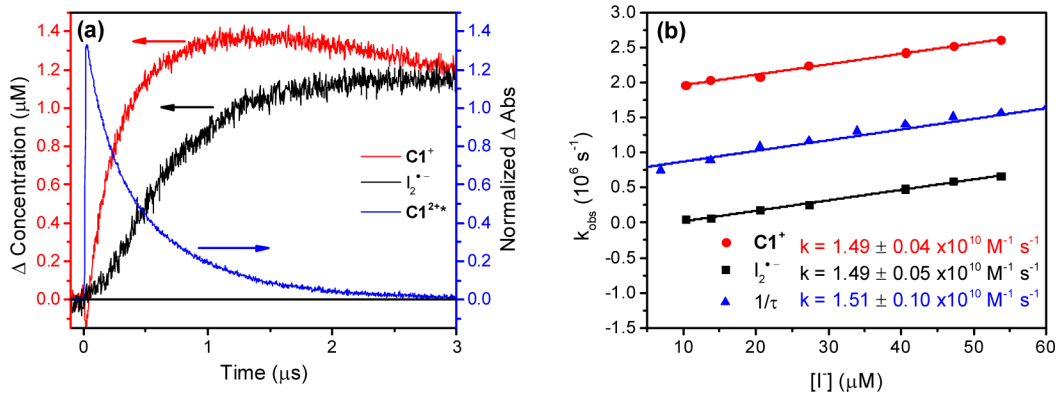

Figure 5. (a) Time dependent concentration changes of $I_2^{\bullet-}$ (black), $\mathbf{C1}^{2+}$ (red) and the excited-state decay (blue). (b). Observed rate constant for the formation of the monoreduced complex and $I_2^{\bullet-}$ at various concentrations of iodide. Measurements were performed at a $\mathbf{C1}^{2+}$ concentration of 10 μM in CH_2Cl_2. The laser fluence was 3 mJ/pulse.

excitation showed two isosbestic points at 402 and 519 nm, Figure S28. Upon the addition of iodide, two new features centered at 400 and 520 nm were observed and assigned to the growth of diiodide, $I_2^{\bullet-}$, and the singly reduced complex ($\mathbf{C1}^{+}$) respectively. The extinction coefficient spectrum of $\mathbf{C1}^{+}$, i.e., $[Ru(dtb)_2(dea^{-})]^{+}$, was obtained by transient absorption measurements after pulsed laser excitation of $\mathbf{C1}^{2+}$ in the presence of tri-*p*-tolylamine (TPA) as a reductive quencher. Subtraction of the known TPA^{+} absorption spectrum yielded the desired spectrum.[16] The $\mathbf{C1}^{+}$ extinction coefficient spectrum showed maxima around 520 and 380 nm with minimal absorbance at 402 nm, Figure S27.

The absorbance spectrum of $I_2^{\bullet-}$ was obtained in CH_2Cl_2 by direct excitation of tetrabutylammonium triiodide and was found to be very similar to the spectrum previously reported in CH_3CN.[17] The $I_2^{\bullet-}$ radical anion has absorption maxima centered at 370 and 750 nm. The rate constant for $I^{\bullet} + I^{-} \rightarrow I_2^{\bullet-}$ in CH_2Cl_2 was determined to be $1.7 \pm 0.2 \times 10^{10}$ M^{-1} s^{-1}, Figures S29–S30. Single wavelength kinetics data obtained at 402 nm reported primarily on the formation of $I_2^{\bullet-}$ while those obtained at 519 nm primarily reported on the monoreduced complex. Figure 4a shows typical data with an initial $\mathbf{C1}^{2+}$ concentration of 70 μM.

Single wavelength transient absorption data were used to determine the rate constant for formation of $\mathbf{C1}^{+}$ and $I_2^{\bullet-}$, $5.9 \pm 0.4 \times 10^{9}$ M^{-1} s^{-1} and $6.2 \pm 0.1 \times 10^{9}$ M^{-1} s^{-1} respectively (Figure 4b and c). Time-resolved PL data collected during the transient absorption experiment yielded a quenching rate constant of $5.5 \pm 0.2 \times 10^{9}$ M^{-1} s^{-1}.

The kinetic measurements were repeated at a lower ruthenium concentration (10 μM). In addition, the absorption changes were converted to concentration changes using Beer's law (Figure 5a). At 10 μM, a larger rate constant for the appearance of $\mathbf{C1}^{+}$, $1.5 \pm 0.04 \times 10^{10}$ M^{-1} s^{-1} and for $I_2^{\bullet-}$, $1.5 \pm 0.05 \times 10^{10}$ M^{-1} s^{-1} were measured, Figure 5. The excited state also yielded a quenching rate constant of $1.5 \pm 0.10 \times 10^{10}$ M^{-1} s^{-1}. Hence the rate constants in these highly ion-paired and unbuffered solutions increased upon decreasing the solution strength.

Competition experiments were performed in which 1 equiv of chloride was initially added to a CH_2Cl_2 solution of $\mathbf{C1}^{2+}$. Iodide was then titrated into the solution and quenching was observed by steady-state PL with a quenching rate constant of $1.9 \pm 0.2 \times 10^{10}$ M^{-1} s^{-1}, Figure 6. This value is similar in magnitude to that determined by the titration of iodide alone, i.e., $2.6 \pm 0.1 \times 10^{10}$ M^{-1} s^{-1}.

Square wave voltammetry of $\mathbf{C1}^{2+}$ and the complex ion-paired with chloride, $[\mathbf{C1}^{2+}, \mathbf{Cl}^{-}]^{+}$, was performed using decamethylferrocene (250 mV vs NHE)[18] as an internal standard, Figure 7.

In a 100 mM $TBAClO_4$ CH_2Cl_2 solution, the $Ru^{III/II}$ potential $E^{o}(\mathbf{C1}^{3+/2+})$ was 1.68 V vs NHE. With the addition of ~5 equiv of chloride, this potential shifted to 1.72 V. The first ligand reduction, $\mathbf{C1}^{2+/+}$, shifted from −0.82 to −0.86 V with the addition of chloride. This gives an estimated increase of ~80 mV in the electrochemical HOMO–LUMO gap. It should be emphasized that unlike iodide, chloride ion-pairing was evident when 100 mM $TBAClO_4$ was present in the CH_2Cl_2 solution as an inert salt (Figures S24–25). The broad shoulder for the $[\mathbf{C1}^{2+}, \mathbf{Cl}^{-}]^{+/0}$ redox chemistry was due to chloride as was demonstrated by control experiments performed in the absence of the metal complex. We note

DOI: 10.1021/jacs.6b11337
J. Am. Chem. Soc. 2016, 138, 16815–16826

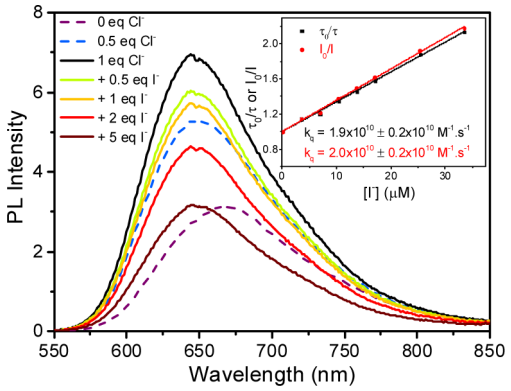

Figure 6. Steady-state PL of $\mathbf{C1}^{2+}$ upon titration of up to 1 equiv of chloride (dashed spectra) followed by the addition of up to 5 equiv of iodide (solid spectra). Inset shows the Stern–Volmer plot for the addition of iodide.

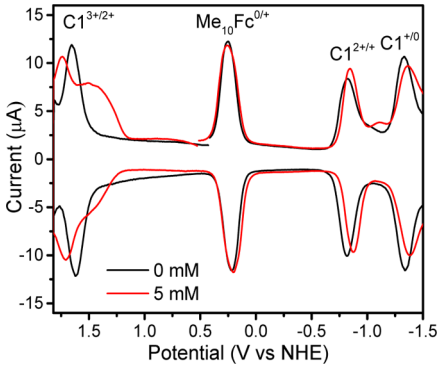

Figure 7. Square wave voltammograms of $\mathbf{C1}^{2+}$ (1.1 mM) in CH_2Cl_2 with 0.1 M $TBAClO_4$ electrolyte before (black) and after (red) the addition of 5 mM chloride.

also that similar chloride redox chemistry has been reported in the literature.[19,20]

The excited-state reduction potentials were calculated from the first $\mathbf{C1}^{2+/+}$ reduction potential and the Gibbs free energy of the excited state, ΔG_{ES}, that was estimated from the x-intercept of a linear extrapolation of the blue edge of the PL corrected spectra,[21] eq 5, where $\mathcal{F}$ is Faraday's constant. The reduction potentials was estimated to be $E°(\mathbf{C1}^{2+*/+}) = +1.27$ and for the chloride ion-pair $E°([\mathbf{C1}^{2+}, \mathbf{Cl}^{-}]^{+*/0}) = +1.25$ vs NHE.

$$E°(\mathbf{C1}^{2+*/+})/\mathcal{F} = E°(\mathbf{C1}^{2+/+})/\mathcal{F} + \Delta G_{ES} \quad (5)$$

DISCUSSION

Control of halide ion-pairing was effected through the design of $\mathbf{C1}^{2+}$, which bears the 4,4′-diethanolamide-2,2′-bipyridine (**dea**) ligand. Ion-pairing between $\mathbf{C1}^{2+}$ and Cl^-, Br^-, and I^- did not result in excited-state quenching. Instead, the ion-paired excited state stored more free energy, was longer lived, and initiated excited-state iodide oxidation through a dynamic mechanism. Static, i.e., nondiffusional, electron transfer between redox active ion-pairs is commonly observed, but dynamic electron transfer is unusual with little if any precedence. This new halide photooxidation mechanism is described below, preceded by a discussion of the nature of the ion-pairs. A systematic analysis of the mechanistic data provides compelling evidence that iodide photooxidation yields an iodide atom and provides new insights into how such ion-pairing influences the thermodynamics for excited-state electron transfer.

Ion-Pair Structure. The **dea** ligand design was inspired by the work of Beer et al., who have previously employed amides for halide recognition. Indeed, ruthenium polypyridyl complexes bearing similar 4,4′-diamide-2,2′-bipyridine ligands displayed halide ion-pairing behavior in DMSO that did not occur in the absence of the amides, highlighting the importance of this functional group for ion-pairing.[6] The spectroscopic data reported herein provides compelling evidence for the presence of a 1:1 $\mathbf{C1}^{2+}$ to halide contact ion-pair. This ion-pair has photophysical properties distinct from the non-ion-paired chromophore.

The ^1H NMR titrations provided insight into the ion-pair equilibrium and the specific halide binding sites (Scheme 1). The ^1H NMR resonance shifts were consistently larger in the lower dielectric constant solvent CH_2Cl_2. The presence of halides induced significant shifts in the proton resonances associated with the **dea** ligand, Table 2. Job plots indicated a 1:1 halide to complex stoichiometry with anion dependent spectral changes. The most pronounced shift induced by chloride was the hydroxyl proton resonance while the most pronounced shift induced by iodide was the amide N–H resonance.

Table 2. Change in ^1H NMR Chemical Shifts upon the Addition of Iodide or Chloride, in Dichloromethane and Acetonitrile

	$H_{3,3'}$	H_{OH}	H_{NH}
Δppm of CH_2Cl_2, I^-	1.05	0.52	1.33
Δppm of CH_2Cl_2, Cl^-	1.42	1.96	1.68
Δppm of CH_3CN, I^-	0.70	0.25	0.92
Δppm of CH_3CN, Cl^-	1.23	1.36	1.36

The halide binding site precludes solvent separation between the halide and the amide hydrogens and leads to the assignment of $[\mathbf{C1}^{2+}, \mathbf{X}^-]^+$ as a *contact ion-pair*, Figure 8. Furthermore, the observed trend in the chemical shifts upon titration are consistent with expectations based on the halide radii. The small size of chloride (r_{ion} 1.81 Å) allows the ethanol side chains to achieve a more favorable geometry in which the hydroxyl H atom points directly toward chloride, whereas the

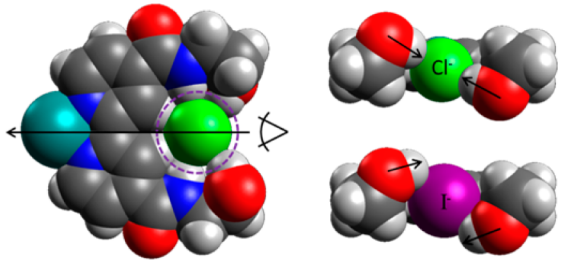

Figure 8. Left-hand side is the proposed structure of $[\mathbf{C1}^{2+}, \mathbf{X}^-]^+$ contact ion-pair with chloride (green sphere) and iodide (purple dashed circle). Color code is blue (nitrogen), blue-green (ruthenium), gray (carbon), red (oxygen) and white (hydrogen). The right-hand side illustrates the difference in H-bonding between the chloride case (green sphere) and iodide case (purple sphere). The arrow in the left image indicates the point of view for the right images. The arrows in the right images emphasize the direction of the O–H bonds. Note that the dtb ligands were omitted for clarity.

DOI: 10.1021/jacs.6b11337
J. Am. Chem. Soc. 2016, 138, 16815–16826

ethylene spacer is not long enough to wrap around the larger iodide (r_{ion} 2.20 Å).[22] This hinders hydrogen binding with iodide as was manifest in the smaller ^{1}H NMR shifts and equilibrium constants than that measured for chloride.

For **C1**$^{2+}$, halide titrations performed in both CH_3CN and CH_2Cl_2 led to an increase in the PL intensity and a blue-shift in the PL maximum. Titrations in CH_2Cl_2 showed complete conversion to the ion-paired species that precluded the determination of the equilibrium binding constant, K_{ip}, values. The PL intensity increases were remarkable for chloride, which approximately doubled the quantum yield. As excited-state quenching was observed with bromide and iodide, the enhanced lifetimes and yields represent best estimates of the 1:1 stoichiometry ion-pairs.

In CH_3CN, the equilibrium binding constant, K_{ip}, determined from both absorbance and PL data increased with the size-to-charge ratio of the halides, $Cl^- > Br^- > I^-$. The excited-state absorption spectra were independent of the identity of the halide or of its presence indicating that the blue shift was not due to localization of the excited state on the **dtb** ligand. In other words, the metal-to-ligand charge-transfer (MLCT) excited-state **C1**$^{2+}$* was well formulated as $[Ru^{III}(dtb)_2(dea^-)]^{2+}$* under all experimental conditions. Interestingly in CH_3CN, a larger K_{ip} for chloride was abstracted from the PL data relative to the absorbance data whereas a smaller one was determined when bromide or iodide were used. These observations indicated that the excited state of **C1**$^{2+}$ binds chloride more strongly than the ground state whereas the opposite was true for bromide and iodide. One might have expected that localization of an electron on the **dea** ligand would result in unfavorable excited-state electrostatics, but this was not the case for chloride and may result from increased planarity of the **dea** ligand that was absent for bromide and iodide due to steric crowding.[23,24]

The increased excited-state lifetime that resulted from ion-pairing can be understood as the result of at least two effects. The blue shift in the PL spectra with ion-pairing indicates an increased ground-excited-state energy gap and a longer lifetime is therefore expected based on Jortner's energy gap law.[25] It is also reasonable to expect that the halide brings the amide moieties into greater planarity with the bipyridine π system, increasing delocalization of the excited electron along the ligand π system.[26,27] This hypothesis is supported by Density Functional Theory (DFT) calculations that predict a decrease in the angle between the amide moiety and the pyridyl rings upon chloride ion-pairing, Figure S31.

Excited-State Ion-Pair Electron-Transfer Mechanism. The experimental data clearly identifies the reaction products as the reduced Ru complex **C1**$^+$ and $I_2^{\bullet-}$. Cage escape yields determined on a nanosecond time scale indicated that these photoproducts were produced with a quantum yield of 0.34. It is worthwhile to consider the possible mechanism(s) for this excited-state iodide oxidation. A static electron-transfer mechanism, involving a nonluminescent ion-pair, was immediately ruled out as the ion-pairs are more highly luminescent and showed no evidence of electron transfer in steady-state quenching experiments. This presumably occurs because the ion-paired iodide is more difficult to oxidize. Hence only dynamic mechanisms were considered and four possibilities are shown in Figure 9.

A "concerted" mechanism has been proposed in thermal stopped-flow iodide oxidation studies by Stanbury and Nord,[28,29] in which electron transfer and I–I bond formation

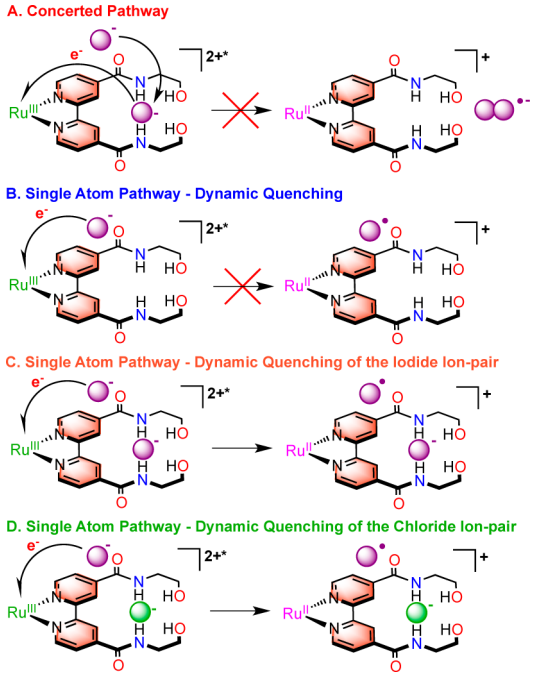

Figure 9. Plausible dynamic quenching of **C1**$^{2+}$* by iodide. The presence of the electron on the dea ligand in **C1**$^{2+}$* and **C1**$^+$ is emphasized by the orange colored bipyridine. Purple spheres represent iodine species whereas green spheres represent chloride. Ancillary **dtb** ligands are omitted for clarity.

occur in one step, Figure 9A. It has also been proposed to be operative in dye-sensitized solar cells. The termolecular nature of the reaction has prompted researchers to speculate that it occurs through ion-paired intermediates. This mechanism has been rigorously tested by quantifying the appearance of the **C1**$^+$ and $I_2^{\bullet-}$ products after pulsed laser excitation. A concerted mechanism cannot be fully ruled out based on kinetic measurements, but is not believed to be operative as is discussed below.

Transient absorption measurements revealed that excited-state electron-transfer rate constants decreased as the solution ionic strength increased, behavior consistent with the reaction of a cationic ion-paired excited state and an iodide donor. For example, with 70 μM **C1**$^{2+}$, the formation of the **C1**$^+$ and $I_2^{\bullet-}$ occurred with second-order rate constants of $6.2 \pm 0.1 \times 10^9$ M^{-1} s^{-1} and $5.9 \pm 0.4 \times 10^9$ M^{-1} s^{-1} respectively, that were within experimental error the same and well below the expected diffusion limit. The excited-state quenching constant was within experimental error the same, consistent with **C1**$^+$ and $I_2^{\bullet-}$ being primary photochemical products. However, the rate constant for the reaction $I^- + I^\bullet \rightarrow I_2^{\bullet-}$ was determined to be $1.7 \pm 0.2 \times 10^{10}$ M^{-1} s^{-1} under these conditions, and hence in the excited-state reaction, the I–I bond formation step may be rate limited by the appearance of iodine atoms. This interpretation was born out in measurements with a much lower 10 μM **C1**$^{2+}$ concentration where excited-state decay and both products occurred with the same rate constant of $1.5 \pm 0.05 \times 10^{10}$ M^{-1} s^{-1}, which is approximately that expected for a diffusion limited reaction. It was previously shown for a family of ruthenium sensitizer that the rate constant for excited-state quenching by iodide ranged from 6.0×10^9 M^{-1} s^{-1} to 6.6×10^{10} M^{-1} s^{-1} in CH_3CN or CH_2Cl_2 solutions.[30,31] Hence the kinetic data are consistent with either a concerted electron-transfer mechanism

DOI: 10.1021/jacs.6b11337
J. Am. Chem. Soc. 2016, 138, 16815–16826

or one that involves iodine atom formation as the rate limiting step.

The concerted mechanism would require I–I bond formation with a freely diffusing iodide and the ion-paired iodide in the $[\mathbf{C1}^{+}, \mathbf{I}^{-}]^{+*}$ excited state. This follows from the quenching data that was consistently first-order in iodide concentration. By analogy, iodide quenching of the chloride ion-paired $[\mathbf{C1}^{2+}, \mathbf{Cl}^{-}]^{+*}$ excited state would yield the iodine monochloride radical, $ICl^{\bullet-}$, whose absorbance should be blue-shifted in respect to $I_2^{\bullet-}$. There was nonetheless no spectroscopic evidence for such interhalogen bond formation. Instead the transient data were fully consistent with the formation of $I_2^{\bullet-}$. This indirect measurement represents the most compelling evidence that the reaction between an ion-paired excited state and iodide generates a single iodine atom.

Two possible iodine atom pathways were considered in Figure 9, one that involved the $\mathbf{C1}^{2+*}$ excited state and the other that involved ion-paired $[\mathbf{C1}^{2+}, \mathbf{X}^{-}]^{+*}$. The former mechanism can be eliminated as the sole electron-transfer process since it would imply decreased reactivity as the iodide concentration increased. Furthermore, chloride ion-paring is stronger in the excited state than in the ground state indicating that dissociation of the ion-pair by light is not operative. Nevertheless, the cage escape yields were less than unity and multiple pathways are possible so a Debye–Hückel analysis was performed at various ionic strengths to distinguish whether the iodide reaction took place with a dicationic or a monocationic excited state.

$$\log(k_q) = k_{q,0} + \frac{2AZ_+Z_-\mu^{1/2}}{1 + \alpha\beta\mu^{1/2}} \tag{6}$$

Eq 6 relates the quenching constant k_q to the ionic strength μ and the charges of the reactants, Z_+Z_-. The identities of the constants are explained in the Experimental Section.[32] A plot of $\log(k_q)$ vs the properly formulated ionic strength revealed a slope of −0.92 that was most consistent with the reaction of iodide and a monocationic ion-paired $[\mathbf{C1}^{2+*}, \mathbf{X}^{-}]^{+}$ species. Furthermore, in the presence of 100 mM $TBAClO_4$, iodide ion-pairing with $C1^{2+}$ was suppressed and there was no evidence for excited-state electron transfer (Figure S22). Therefore, pathway B is not operative and the mechanism is identified as one in which iodide reacts with an ion-paired excited state, pathways C and D in Figure 9.

Thermodynamic Considerations. It remains unclear why electron transfer was only observed from the ion-paired excited state and only in dichloromethane. Prior work has shown that iodide oxidation occurs with rate constants greater than 10^9 M^{-1} s^{-1} for related dicationic MLCT excited states in CH_3CN solutions with similar driving forces.[33] Yet this was not observed here, requiring a deeper look into the thermodynamics for ion-pair formation and excited-state iodide oxidation.

The significant blue shift in the PL spectra that occurs with halide ion-pairing suggests that the excited state would be a stronger oxidant than the non-ion-paired excited state, but electrochemical data reveals that this is almost equally offset by a shift in the ground-state reduction potential. The inherent uncertainties in the free energy stored in the excited state, and its small dependency on the halide identity lead to the conclusion that the oxidation potential of $[\mathbf{C1}^{2+}, \mathbf{X}^{-}]^{+*}$ and $\mathbf{C1}^{2+*}$ are within experimental error the same, 1.26 ± 0.2 V, and cannot account for the remarkable reactivity turn-on induced by ion-pairing, Table 3.

Table 3. Electrochemical and Free Energy Data for the Photooxidation of Iodide by $\mathbf{C1}^{2+}$

	ΔG_{ES} (eV)[a]	$E°$ ($\mathbf{C1}^{2+/+}$) (V vs NHE)	$E°$ ($\mathbf{C1}^{2+*/+}$) (V vs NHE)	ΔG_w (eV)[b]	ΔG_{rxn} (eV)[c]
$\mathbf{C1}^{2+}$	2.09	−0.82	1.27	−0.39	−0.43
$[\mathbf{C1}, \mathbf{Cl}^{-}]^{+}$	2.11	−0.86	1.25	−0.25	−0.27

[a]Extrapolated from the corrected PL spectra as the abscissa intercept. [b]Calculated from eq 8 assuming an iodide position of 7.2 Å from the Ru center. [c]From eq 7.

The Gibbs free energy change for iodide oxidation, $\Delta G_{rxn,}$ is related to the formal reduction potentials and the Coulombic work term, ΔG_w, associated with the change in donor–acceptor electrostatic interactions upon electron transfer, eq 7 where $\mathcal{F}$ is Faraday's constant.[34−36] The ΔG_w term is often neglected as in polar solvents the contributions are generally small. However, this is not necessarily the case in organic solvents where ion-pairing is evident.

$$\Delta G_{rxn} = E°(C1^{2+*/+})/\mathcal{F} - E°(I^{\bullet/-})/\mathcal{F} + \Delta G_w \tag{7}$$

$$\Delta G_w = \frac{k_e}{\varepsilon}\Delta \sum_{j=1} \frac{Z_I Z_j}{r_{Ij}} \tag{8}$$

The work term has been calculated directly through eq 8, where k_e is Coulomb's constant, ε is the relative permittivity of CH_2Cl_2 (~9), Z_I is the charge of iodide, Z_j is the partial charge of atom j of $\mathbf{C1}^{2+}$ or $[\mathbf{C1}^{2+}, \mathbf{Cl}^{-}]^{+}$, and r_{Ij} is the distance between the iodide and atom j of $\mathbf{C1}^{2+}$ or $[\mathbf{C1}^{2+}, \mathbf{Cl}^{-}]^{+}$. Since the iodine atom is not charged, the Coulombic potential energy after the electron transfer is zero.

To our knowledge previous studies of excited-state electron transfer have not attempted to assign partial charges to each atom. Instead, the overall charge was placed at the center of mass of each ion.[34−36] This simplified approach reveals a $-\Delta G_w$, and hence an increased driving force, of 390 mV for $\mathbf{C1}^{2+}$ and 250 mV for $[\mathbf{C1}^{2+}, \mathbf{Cl}^{-}]^{+}$, Table 3. This relative permittivity would give rise to work term that are almost 4 times smaller for CH_3CN (ε = 37.5) than for CH_2Cl_2 (ε = 8.9) which begins to explain why no such quenching was observed in CH_3CN. These values were calculated at an r_{Ij} = 7.2 Å, yet the point charge approximation is most valid when the ions are much further away. As an iodide ion and the complex diffuse toward each other, the atomic contours of the electrostatic fields must begin to play a critical role.

To gain insights into the electrostatic interactions of the individual atoms in $\mathbf{C1}^{2+}$ and $[\mathbf{C1}^{2+}, \mathbf{Cl}^{-}]^{+}$, the natural atomic charge of each individual atom was calculated through natural bond order analysis.[37] Shown in Figure 10 are contour plots of the calculated work terms over the plane containing the **dea** ligand in both the absence and presence of an ion-paired chloride.

Figure 10A shows the Coulombic incentive for ion-pair formation in the proposed binding site. Indeed, the values range from −100 meV when the halide anion was located 20 Å from the ruthenium center and reached a value close to −500 meV in the binding site provided by the **dea** ligand. Furthermore, the magnitude of the Coulombic work term was substantially decreased at all locations after ion-pairing

DOI: 10.1021/jacs.6b11337
J. Am. Chem. Soc. 2016, 138, 16815–16826

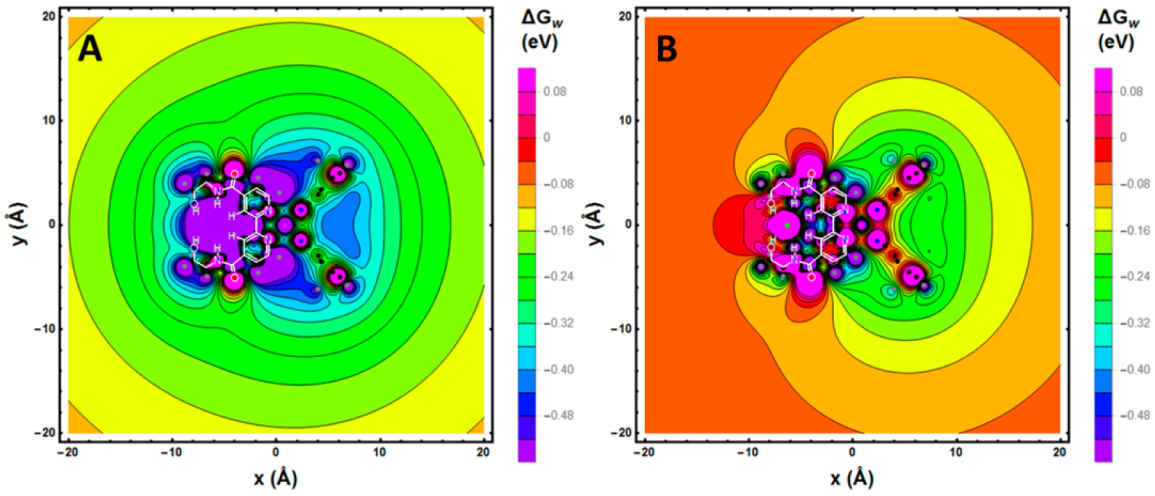

Figure 10. Contour plots of the calculated Coulombic work term, ΔG_w, in eV over the plane containing the **dea** ligand in the absence, A, and presence, B, of the chloride ion-pair. All atoms within 1 Å of this plane are shown as small colored dots. The **dea** ligand is superimposed in white.

induced a unit decrease in the overall complex charge. Interestingly a halide anion approaching the chloride-paired **dea** binding site from a distance up to 20 Å gives rise (up to −240 meV) to only unfavorable work terms while approach on the **dtb** side gives rise to favorable work terms and hence less Coulombic repulsion. A preference for halide association remote to the ion-paired dea ligand should be even more pronounced in the MLCT excited state and suggests that iodide oxidation occurs in the dark green regions near the **dtb** ligands, Figure 10B.

These electrostatic considerations do not address the questions raised at the beginning of this section. Indeed, they indicate that the thermodynamic driving force for iodide photooxidation decreased upon ion-pairing which is at odds with the turn-on in reactivity. To explain this phenomenon, we propose that ion-pairing competes kinetically with electron transfer *and* an ion-paired iodide stabilized in the **dea** ligand that is no longer a sufficiently potent reductant to react with the excited state. The kinetics for ion-pairing are unknown, but quenching rate constants of $\sim 6 \times 10^9$ M^{-1} s^{-1} imply a barrier to electron transfer that the electrostatically driven ion-paring could outcompete. The free energy change for ion-pairing is tremendous with K_{ip} values of 10^4 M^{-1} in CH_3CN and immeasurably high $>10^6$ M^{-1} in dichloromethane. These values do not directly address the formal $E°(I^{\bullet/-})$ reduction potential of the ion-paired iodide as it is conceivable that the Ru complex is stabilized to such a great extent that the iodide is destabilized. However, this seems highly unlikely when one considers the magnitude of the equilibrium constants and the Lewis basic nature of iodide that should render it more difficult to oxidize in the ion-pair.

A conclusion therefore is that $\mathbf{C1}^{2+*}$ traps iodide on the **dea** ligand and thus prevents its oxidation. Such behavior is ideal for iodide sensing as K_{ip} is large and the concomitant blue shift of the photoluminescence spectra is useful for ratiometric sensing. The fact that no excited-state quenching of the ion-pair is observed is not optimal for solar energy conversion applications where iodide oxidation is desired. For dye-sensitized solar cells or HI splitting applications, ion-pairing maintains an iodide near the photosensitizer that influences the work terms for electron transfer and may one day enable iodide photooxidation without diffusion. The observed ion-pairing consumes an iodide ion and decreases the driving force for electron transfer. Hence, ligands that destabilize iodide yet retain or increase the Coulombic attraction charge are expected to be the most ideal when photoredox chemistry is desired.

CONCLUSIONS

In this work, the interaction of a ruthenium polypyridyl complex bearing a 4,4′-diethanolamide-2,2′-bipyridine ligand, with chloride, bromide, and iodide was studied in both acetonitrile and dichloromethane. A 1:1 ion-paired halide complex was identified and characterized by standard spectroscopic and electrochemical techniques. The use of DFT computations to quantify the work terms for electron transfer in all the atoms of the complex provided electrostatic contour plots for the first time. The ion-pair formed was shown to photooxidize iodide, whereas the non-ion-paired species did not. This reactivity was not simply due to the ion-paired complex being a stronger oxidant or having a longer excited state lifetime. Instead, it was concluded that iodide ions were trapped and stabilized more rapidly than excited-state electron transfer. Ligands such as **dea** are desirable for anion sensing, while alternative ligands that provide Coulombic attraction yet destabilize the anion are more suitable for photoredox chemistry and solar energy conversion applications.

EXPERIMENTAL SECTION

Materials. Sulfuric acid (H_2SO_4, Fisher, 98%, Certified ACS Plus), methanol (Fisher, Certified ACS), chloroform (Fisher, Certified ACS), ethanolamine (Sigma-Aldrich, ≥98%), acetone (Sigma-Aldrich, Certified ACS), acetonitrile (CH_3CN, Burdick and Jackson, 99.98%), and dichloromethane (CH_2Cl_2, Burdick and Jackson, 99.98%) were used as received. Argon gas (Airgas, 99.998%) was passed through a Drierite drying tube before use. Ammonium hexafluorophosphate (NH_4PF_6, Sigma-Aldrich, ≥98%), tetrabutylammonium chloride (TBACl, Sigma-Aldrich, purum ≥97%), tetrabutylammonium bromide (TBABr, Acros Organics, 99+%), tetrabutylammonium iodide (TBAI, Sigma-Aldrich, ≥99%), tetrabutylammonium perchlorate ($TBAClO_4$, Sigma-Aldrich, for electrochemical analysis, ≥99%), tetrabutylammonium triiodide ($TBAI_3$ Sigma-Aldrich, ≥97%), ruthenium trichloride hydrate (Oakwood Chemicals, 97%), and tri-*p*-tolylamine (TCI America, ≥98%) were used as received. NMR solvents were purchased from Cambridge Isotope Laboratories, Inc. $Ru(dtb)_2Cl_2 \cdot 2H_2O$ and 2,2′-bipyridine-4,4′-dicarboxylic acid were synthesized according to a literature procedure.[38] All solutions were

DOI: 10.1021/jacs.6b11337
J. Am. Chem. Soc. 2016, 138, 16815−16826

sparged with argon for at least 30 min before all titration and transient absorption experiments.

Synthesis. *4,4′-Dimethylester-2,2′-bipyridine.* The 4,4′-dimethylester-2,2′-bipyridine was synthesized by a modified literature procedure.[12] Briefly, to a mixture of 10 mL of H_2SO_4 and 90 mL of methanol was added 5.0 g (20.5 mmol) of 2,2′-bipyridine-4,4′-dicarboxylic acid. The mixture was refluxed until there was no visible solid. The cooled pink solution was poured into chloroform and extracted with water until no color was apparent. The organic fraction was then evaporated under reduced pressure to yield 5.3 g (95%) of a microcrystalline white solid. ^{1}H NMR ($CDCl_3$, 400 MHz): 8.96 (2H, dd), 8.86 (2H, dd), 8.80 (2H, dd), 4.00 (6H, s).

*4,4′-Diethanolamide-2,2′-bipyridine, (**dea**).* To 1.0 g (3.7 mmol) of 4,4′-dimethylester-2,2′-bipyridine in 20 mL of methanol was added 5 mL (5.1 g, 83 mmol) of ethanolamine. The mixture was refluxed for 4 h. After cooling, ∼ 25 mL of acetone was added to the resulting mixture that was then filtered on a sintered glass frit. The precipitate was washed with a copious amount of acetone and dried in an evacuated oven overnight at 150 °C to yield 1.1 g (92%) of a white powder. ^{1}H NMR (DMSO-d_6, 600 MHz): 8.95 (2H, t), 8.87 (2H, d), 8.81 (2H, s), 7.87 (2H, dd), 4.8 (2H, t), 3.55 (4H, m), 3.38 (4H, m). ^{13}C NMR (DMSO-d_6, 600 MHz): 164.70, 155.52, 150.05, 142.98, 122.00, 118.30, 59.51, 42.37.

*[Ru(dtb)$_2$(dea)](PF$_6$)$_2$, (**C1**$^{2+}$).* To a 10 mL glass microwave vial was added 100 mg (0.14 mmol) of $Ru(dtb)_2Cl_2{\cdot}2H_2O$, 49 mg (0.15 mmol) of **dea**, and ∼5 mL of water. The mixture was heated under microwave radiation by an Anton Paar Monowave 300 at 150 °C for 10 min. The resulting mixture was filtered on a sintered glass frit. The filtrate was then treated with an excess of aqueous NH_4PF_6 and precipitated an orange solid that was filtered on a sintered glass frit and washed with a copious amount of water. The precipitate was then dried under vacuum to give the desired product in a 78% yield. ^{1}H NMR (CD_2Cl_2, 600 MHz): 8.88 (2H, s), 8.27 (4H, d), 7.82 (2H, dd), 7.77 (2H, d), 7.57 (2H, d), 7.55 (2H, d), 7.51 (2H, t), 7.46 (2H, dd), 7.44 (2H, dd), 3.78 (4H, m), 3.58 (4H, m), 2.72 (2H, bs) 1.42 (18H, s), 1.40 (18H, s). ^{13}C NMR ($CDCl_3$, 600 MHz): 164.38, 163.14, 163.05, 157.35, 156.32, 156.18, 151.54, 150.75, 150.52, 143.08, 125.97, 125.78, 125.50, 121.72, 120.79, 61.46, 50.46, 43.28, 35.54, 35.52, 30.63, 29.99, 29.95. Elem anal. Calcd for $RuC_{52}H_{66}N_8O_4P_2F_{12}$ (1258.13): C, 49.64; H, 5.29; N, 8.91. Found: C, 48.23; H, 5.21; N, 8.60. HRMS (ESI-MS) m/z: $[M]^{2+}$ Calcd for $C_{52}H_{66}N_8O_4{}^{96}RuPF_6$ 1107.3925; Found 1107.3963.

Nuclear Magnetic Resonance. Characteristic NMR spectra were obtained at room temperature on a Bruker Avance III 400 or 600 MHz spectrometer. Solvent residual peaks were used as internal standards for ^{1}H (δ = 7.26 ppm for $CDCl_3$, 2.50 ppm for DMSO) and ^{13}C (δ = 77.16 ppm for $CDCl_3$, 39.52 ppm for DMSO) chemical shift referencing. NMR spectra were processed using MNOVA.

Mass Spectrometry. Samples were analyzed with a hybrid LTQ FT (ICR 7T) (ThermoFisher, Bremen, Germany) mass spectrometer. Samples were introduced via a microelectrospray source at a flow rate of 3 μL/min. Xcalibur (ThermoFisher, Breman, Germany) was used to analyze the data. Each mass spectrum was averaged over 200 time domains. Electrospray source conditions were set as spray voltage 4.7 kV, sheath gas (nitrogen) 3 arb, auxiliary gas (nitrogen) 0 arb, sweep gas (nitrogen) 0 arb, capillary temperature 275 °C, capillary voltage 35 V and tube lens voltage 110 V. The mass range was set to 150−2000 m/z. All measurements were recorded at a resolution setting of 100 000. Solutions were analyzed at 0.1 mg/mL or less based on responsiveness to the ESI mechanism. Low-resolution mass spectrometry (linear ion trap) provided independent verification of molecular weight distributions.

Elemental Analysis. Elemental analysis was performed by Atlantic Microlabs, LLC.

UV−Vis Absorption. UV−vis absorption spectra were recorded on a Varian Cary 60 UV−vis spectrophotometer with a resolution of 1 nm. The extinction coefficients were determined by diluting a stock solution of complex **C1**$^{2+}$ and represent averages of at least three independent measurements.

Steady-State PL. Steady-state PL spectra were recorded on a Horiba Fluorolog 3 fluorimeter and corrected by calibration with a standard tungsten-halogen lamp. Samples were excited at 450 nm. The intensity was integrated for 0.1 s at 1 nm resolution and averaged over 3 scans. The PL quantum yields were measured by the optically dilute method using $[Ru(bpy)_3][PF_6]_2$ in acetonitrile (Φ = 0.062) as a quantum yield standard.[39]

Time-Resolved Photoluminescence. Time-resolved PL data were acquired on a nitrogen dye laser with excitation centered at 445 nm. Pulsed light excitation was achieved with a Photon Technology International (PTI) GL-301 dye laser that was pumped by a PTI GL-3300 nitrogen laser. The PL was detected by a Hamamatsu R928 PMT optically coupled to a ScienceTech Model 9010 monochromator terminated into a LeCroy Waverunner LT322 oscilloscope. Decays were monitored at the PL maximum and averaged over 180 scans. Nonradiative and radiative rate constants were calculated from the quantum yields, $\Phi = k_r/(k_r + k_{nr})$ and lifetimes, $\tau = 1/(k_r + k_{nr})$.

Electrochemistry. Square wave voltammetry was performed with a BASi Epsilon potentiostat in a standard three-cell in CH_2Cl_2 electrolytes. The cells consisted of a platinum working electrode and a platinum mesh as an auxiliary electrode. A nonaqueous silver/silver chloride electrode (Pine) was used as a reference electrode that was referenced to an internal decamethylferrocene ($Me_{10}Fc$) standard (250 mV vs NHE).[18]

Halide Titrations. UV−vis, PL, and time-resolved measurements were performed in CH_2Cl_2 or CH_3CN using 10 μM of **C1**$^{2+}$.Titration measurements were performed for each of the spectroscopies with TBACl, TBABr, or TBAI through additions of 0.25 equiv. Throughout all titrations the concentration of **C1**$^{2+}$ remained unchanged. In order to do so, a stock solution of **C1**$^{2+}$ with an absorbance of ∼0.1 at 450 nm in the desired solvent was prepared. The stock solution was transferred into a spectrophotometric quartz cuvette (5 mL). A titration solution was then prepared with 25 mL of the **C1**$^{2+}$ stock solution. TBACl, TBABr, or TBAI were added to the stock solution to obtain the desired concentration of halide. These solutions were then titrated to the quartz cuvette.

The ^{1}H NMR titrations were performed using Bruker Avance III 500 MHz spectrometer equipped with a broadband inverse (BBI) probe using 1 mM ruthenium complex in 600 μL of deuterated solvent and 0.25 equiv additions of TBACl or TBAI were added in 10 μL additions. The ruthenium concentration was kept unchanged through preparation of a titration solution that contained both **C1**$^{2+}$ and the desired halide. Each spectrum was averaged over 16 scans.

Data analysis for all experiments was performed using OriginLab, version 9.0. Data fitting was preformed using a Levenberg−Marquardt iteration method. Benesi−Hildebrand type analysis was performed in Mathematica, version 10.

Transient Absorption. Nanosecond transient absorption measurements were acquired on a setup published previously.[40] Briefly, a Q-switched, pulsed Nd:YAG laser (Quantel USA (BigSky) Brilliant B 5−6 ns full width at half-maximum (fwhm), 1 Hz, ∼ 10 mm in diameter) doubled to 532 nm. The laser irradiance at the sample was attenuated to 3 mJ/pulse. The probe lamp consisted of a 150 W xenon arc lamp and was pulsed at 1 Hz with 70 V during the experiment. Signal detection was achieved using a monochromator (SPEX 1702/04) optically coupled to an R928 photomultiplier tube (Hamamatsu) at a right angle to the excitation laser. Transient data were acquired with a computer-interfaced digital oscilloscope (LeCroy 9450, Dual 330 MHz) with an overall instrument response time of ∼10 ns. An average of 30 laser pulses was acquired averaged at each wavelength of interest over the 370−800 nm range. Intervals of 10 nm were used for wavelength between 370 and 600 nm and intervals of 20 nm were used between 600 and 800 nm. Time-resolved PL data were also acquired at the same laser intensity at 532 nm.

Diiodide Extinction Coefficient. The extinction coefficient for diiodide in CH_2Cl_2 was calculated from the transient absorption spectra of a 4 μM $TBAI_3$, 20 μM TBAI solution. A tripled Nd:YAG laser (355 nm) was used to excite the triiodide that produced 1 equiv of iodine atoms and 1 equiv of $I_2^{\bullet-}$ anions, eq 9. The produced iodine atoms further react with the I^- anions to produce $I_2^{\bullet-}$, eq 10.

DOI: 10.1021/jacs.6b11337
J. Am. Chem. Soc. 2016, 138, 16815−16826

Therefore, the overall reaction involves the loss of 1 equiv of triiodide and the gain of 2 equiv of $I_2^{\bullet-}$, eq 11. Immediately after laser excitation (~30 ns) the observed products are 1 equiv of iodine atoms and 1 equiv of I^-, eq 9. After 10 μs the produced iodine atoms have fully reacted to form a second equivalent of $I_2^{\bullet-}$. The transient absorbance spectrum at 30 ns then is the linear combination of the loss of triiodide and the diiodide produced, eq 11, and the TA spectrum at 10 μs is the linear combination of the loss of triiodide and the 2 equiv of diiodide produce, eq 12. Solving the equations for the absorbance of I_3^- and $I_2^{\bullet-}$ and utilizing the known extinction coefficient for I_3^- allows the extinction coefficient of $I_2^{\bullet-}$ to be calculated, eq 13–15. The calculated extinction coefficient of diiodide is shown in Figure S27.

$$I_3^- + h\nu\ (355\text{nm}) \rightarrow I^\bullet + I_2^{\bullet-} \quad (9)$$

$$I^\bullet + I^- \rightarrow I_2^{\bullet-} \quad (10)$$

$$I_3^- + I^- \rightarrow 2I_2^{\bullet-} \quad (11)$$

$$\text{Abs}(I_3^-) = (\mathbf{2}) - 2 \times (\mathbf{1}) \quad (12)$$

$$\text{Abs}(I_2^{\bullet-}) = (\mathbf{2}) - (\mathbf{1}) \quad (13)$$

$$[I_3^-] = \text{Abs}(I_3^-)/\varepsilon(I_3^-) = [I_2^{\bullet-}] \quad (14)$$

$$\varepsilon(I_2^{\bullet-}) = \text{Abs}(I_2^{\bullet-})/[I_2^{\bullet-}] \quad (15)$$

Diiodide Formation Rate Constant. Separate CH_2Cl_2 solutions of $TBAI_3$ (5 μM) in a quartz cuvette and TBAI (0.67 mM) in a 20 mL scintillation vial were prepared. Approximately 1 equiv, 40 μL, aliquots of the I^- solution were added to the triiodide solution to a total of 4 equiv of iodide. The formation of $I_2^{\bullet-}$ after excitation by a tripled Nd:YAG laser (355 nm) was monitored at 410 nm, near an isosbestic point between the absorbance of $I_2^{\bullet-}$ and triiodide. The growth of the diiodide transient signal was well modeled by a single exponential function which yielded the observed formation rate. A second-order rate constant for diiodide formation was then calculated from the slope of the observed rate constants vs the iodide concentration. This procedure was repeated at $TBAClO_4$ concentrations of 1, 10, and 100 mM.

Determination of the Reduced Complex Extinction Coefficient. The absorption spectrum of the singly reduced complex ($\mathbf{C1}^+$) was determined using a procedure adapted from literature.[16] A 10 μM solution of $\mathbf{C1}^{2+}$ with 10 mM tri-*p*-tolylamine (TPA) was irradiated with 532 nm light (1.5 mJ/cm^2). Laser excitation of $\mathbf{C1}^{2+}$ resulted in electron transfer from the TPA to $\mathbf{C1}^{2+}$*. Transient absorption spectra were recorded, normalized at 680 nm, and the normalized spectrum of the oxidized TPA was subtracted from it to give the difference spectrum between the reduced $\mathbf{C1}^+$ and the ground state. The concentration of reduced complex formed was calculated as the extinction coefficient of the oxidized TPA is known.[16] Division of the difference spectrum by the concentration of reduced complex gave the delta extinction coefficient. Linear addition of this delta extinction coefficient to the ground-state $\mathbf{C1}^{2+}$ extinction coefficient yielded the reduced complex extinction coefficient, Figure S27.

Spectral Modeling. Transient absorption spectra of $\mathbf{C1}^{2+}$ in the presence of 4 equiv of iodide resulted in the formation of the reduced complex and diiodide. At any given time, the spectra consisted of the ground-state loss, excited states, the reduced compound, and diiodide, eq 16. The kinetics monitored in the 380–560 nm range wavelength range were modeled through use of the ground state ($\mathbf{C1}^{2+}$) and reduced complex ($\mathbf{C1}^+$) extinction coefficients and the absorbance difference between the excited state and ground state. This allowed the formation of diiodide and the reduced compound to be analyzed as concentration instead of absorbance.

$$\Delta\text{Abs} = \text{Abs}(\mathbf{C1}^{2+*}) - \text{Abs}(\mathbf{C1}^{2+}) + \text{Abs}(\mathbf{C1}^+) + \text{Abs}(I_2^{\bullet-}) \quad (16)$$

Cage Escape Yield. Cage escape yields of the photoinduced iodide oxidation by $\mathbf{C1}^{2+}$ were determined through transient absorption experiments utilizing eqs 17 and 18. Actinometry with a $Ru(bpy)_3^{2+}$ standard was performed between each sample measurement, assuming a unity quantum yield of intersystem crossing to the ^{3}MLCT excited-state. The $\Delta\varepsilon_{450}$ between the ground-state $Ru(bpy)_3^{2+}$ and the excited-state $Ru(bpy)_3^{2+*}$ was -1.5×10^4 M^{-1} cm^{-1},[41] and $\Delta\varepsilon_{520}$ between the ground-state $\mathbf{C1}^{2+}$and the reduced $\mathbf{C1}^+$ was 1.25×10^4 M^{-1} cm^{-1} for $\mathbf{C1}^{2+}$. The slope of a plot of ϕ vs % of PL quenched gave the cage escape yield.[32]

$$\Phi_{CE} = \phi \frac{1}{\%\text{PL quenched}} \quad (17)$$

$$\phi = \frac{\left(\frac{\Delta A_{\lambda 1}}{\Delta \varepsilon_{\lambda 1}}\right)_{C1}}{\left(\frac{\Delta A_{\lambda 2}}{\Delta \varepsilon_{\lambda 2}}\right)_{Ru(bpy)_3}} \frac{(1 - 10^{-A_{532}})_{Ru(bpy)_3}}{(1 - 10^{-A_{532}})_{C1}} \quad (18)$$

Debye–Hückel Analysis. Quenching rates constants from Stern–Volmer analysis were measured with solutions whose ionic strength varying from 0 to 1 mM $TBAClO_4$. The quenching rate constant was found to be dependent on ionic strength, a trend that was analyzed by the extended Debye–Hückel theory according to eq 6.[32] In this equation, μ is the ionic strength, A and β are constants (taken to be 15.3 L$^{1/2}$ mol$^{1/2}$, and 1.02×10^{-8} L$^{1/2}$ mol$^{1/2}$, respectively),[42] α is the effective size parameter, here assumed to be 5.5 Å, $k_{q,0}$ is the quenching constant at $\mu = 0$, and Z_+ and Z_- are the charges of the two species involved in the quenching process. Plotting $\log(k_q)$ vs $(2A\mu^{1/2})/(1 + \alpha\beta\mu^{1/2})$ gives a line with a slope equal to the product of Z_+ and Z_-.[32]

Density Functional Theory. Quantum mechanical calculations were carried out using the Gaussian 09 program package.[43] The structure of $\mathbf{C1}^{2+}$ was optimized to a minimum energy and frequency calculations were performed to verify there were no imaginary frequencies. All calculations utilized the B3LYP functional[44−47] with the 6-311++G**[48] basis set applied to chloride, LANL2DZ[49−51] with an added f-polar function applied to ruthenium,[52] and 6-311G*[53] applied to all other elements. Parameters for the LANL2DZ basis set were obtained from the ESML basis set exchange.[54,55] Second-order perturbations analysis of intermolecular interactions and of natural atomic charges used for Coulombic work term calculations were performed with the NBO 3 program, as implemented in the Gaussian software package.[56−63] All calculations were performed in the gas phase and an ultrafine integration grid was used for all calculations. When convergence was not otherwise achieved, two quadratic convergence steps were added through the SCF = XQC command.

■ ASSOCIATED CONTENT

Supporting Information

The Supporting Information is available free of charge on the ACS Publications website at DOI: 10.1021/jacs.6b11337.

^{1}H, ^{13}C NMR and high resolution mass spectra of **dea** and $\mathbf{C1}^{2+}$; UV–vis, PL and ^{1}H NMR titrations in $C(H_3/D_3)CN$ and $C(H_2/D_2)Cl_2$ as well as Debye–Hückel analysis, cage escape yield, and spectra used for modeling (PDF)

■ AUTHOR INFORMATION

Corresponding Author

*gjmeyer@email.unc.edu

ORCID

Ludovic Troian-Gautier: 0000-0002-7690-1361

Gerald J. Meyer: 0000-0002-4227-6393

Notes

The authors declare no competing financial interest.

■ ACKNOWLEDGMENTS

L.T.-G. acknowledges the Belgian American Educational Foundation (B.A.E.F) for his postdoctoral fellowship. W.B.S.

acknowledges the National Science Foundation Graduate Research Fellowship Program (Grant DGE-1650116). All authors acknowledge support by a grant from the Division of Chemical Sciences, Office of Basic Energy Sciences, Office of Energy Research, U.S. Department of Energy (Grant DE-SC0013461).

REFERENCES

(1) Lakowicz, J. R. *Principles of Fluorescence Spectroscopy*; Plenum Press: New York, 1983.
(2) Winstein, S.; Clippinger, E.; Fainberg, A. H.; Robinson, G. C. *J. Am. Chem. Soc.* **1954**, *76*, 2597−2598.
(3) Sadek, H.; Fuoss, R. M. *J. Am. Chem. Soc.* **1954**, *76*, 5897−5901.
(4) Sadek, H.; Fuoss, R. M. *J. Am. Chem. Soc.* **1954**, *76*, 5905−5909.
(5) Marcus, Y.; Hefter, G. *Chem. Rev.* **2006**, *106*, 4585−4621.
(6) Szemes, F.; Hesek, D.; Chen, Z.; Dent, S. W.; Drew, M. G. B.; Goulden, A. J.; Graydon, A. R.; Grieve, A.; Mortimer, R. J.; Wear, T.; Weightman, J. S.; Beer, P. D. *Inorg. Chem.* **1996**, *35*, 5868−5879.
(7) Beer, P. D.; Fletcher, N. C.; Wear, T. *Polyhedron* **1996**, *15*, 1339−1347.
(8) Beer, P. D.; Dent, S. W.; Wear, T. J. *J. Chem. Soc., Dalton Trans.* **1996**, *1*, 2341−2346.
(9) Beer, P. D.; Dent, S. W.; Hobbs, G. S.; Wear, T. J. *Chem. Commun.* **1997**, *1*, 99−100.
(10) Beer, P. D.; Szemes, F.; Balzani, V.; Salà, C. M.; Drew, M. G. B.; Dent, S. W.; Maestri, M. *J. Am. Chem. Soc.* **1997**, *119*, 11864−11875.
(11) Uppadine, L. H.; Beer, P. D.; Drew, M. G. B. *Chem. Commun.* **2001**, *3*, 291−292.
(12) Ciana, L. D.; Dressick, W. J.; Von Zelewsky, A. *J. Heterocycl. Chem.* **1990**, *27*, 163−165.
(13) Benesi, H. A.; Hildebrand, J. H. *J. Am. Chem. Soc.* **1949**, *71*, 2703−2707.
(14) Ward, W. M.; Farnum, B. H.; Siegler, M.; Meyer, G. J. *J. Phys. Chem. A* **2013**, *117*, 8883−8894.
(15) Le, V. H.; Yanney, M.; McGuire, M.; Sygula, A.; Lewis, E. A. *J. Phys. Chem. B* **2014**, *118*, 11956−11964.
(16) Dimarco, B. N.; O'Donnell, R. M.; Meyer, G. J. *J. Phys. Chem. C* **2015**, *119*, 21599−21604.
(17) Gardner, J. M.; Abrahamsson, M.; Farnum, B. H.; Meyer, G. J. *J. Am. Chem. Soc.* **2009**, *131*, 16206−16214.
(18) Noviandri, I.; Brown, K. N.; Fleming, D. S.; Gulyas, P. T.; Lay, P. A.; Masters, A. F.; Phillips, L. *J. Phys. Chem. B* **1999**, *103*, 6713−6722.
(19) Kolthoff, I. M.; Coetzee, J. F. *J. Am. Chem. Soc.* **1957**, *79*, 1852−1858.
(20) Du, J.; Chen, Z.; Chen, C.; Meyer, T. J. *J. Am. Chem. Soc.* **2015**, *137*, 3193−3196.
(21) Adamson, A. W.; Namnath, J.; Shastry, V. J.; Slawson, V. *J. Chem. Educ.* **1984**, *61*, 221.
(22) Shannon, R. D. *Acta Crystallogr., Sect. A: Cryst. Phys., Diffr., Theor. Gen. Crystallogr.* **1976**, *32*, 751−767.
(23) Alford, P. C.; Cook, M. J.; Lewis, A. P.; McAuliffe, G. S. G.; Skarda, V.; Thomson, A. J.; Glasper, J. L.; Robbins, D. J. *J. Chem. Soc., Perkin Trans. 2* **1985**, *1*, 705−709.
(24) Hahn, U.; Vögtle, F.; De Paoli, G.; Staffilani, M.; De Cola, L. *Eur. J. Inorg. Chem.* **2009**, *2009*, 2639−2646.
(25) Englman, R.; Jortner, J. *Mol. Phys.* **1970**, *18*, 145−164.
(26) Gu, J.; Yan, Y.; Helbig, B. J.; Huang, Z.; Lian, T.; Schmehl, R. H. *Coord. Chem. Rev.* **2015**, *282*−*283*, 100−109.
(27) O'donnell, R. M.; Sampaio, R. N.; Li, G.; Johansson, P. G.; Ward, C. L.; Meyer, G. J. *J. Am. Chem. Soc.* **2016**, *138*, 3891−3903.
(28) Stanbury, D. M.; Wilmarth, W. K.; Khalaf, S.; Po, H. N.; Byrd, J. E. *Inorg. Chem.* **1980**, *19*, 2715−2722.
(29) Nord, G. *Comments Inorg. Chem.* **1992**, *13*, 221−239.
(30) Farnum, B. H.; Gardner, J. M.; Marton, A.; Narducci-Sarjeant, A. A.; Meyer, G. J. *Dalt. Trans.* **2011**, *40*, 3830.
(31) Farnum, B. H.; Jou, J. J.; Meyer, G. J. *Proc. Natl. Acad. Sci. U. S. A.* **2012**, *109*, 15628−15633.
(32) Clark, C. D.; Hoffman, M. Z. *J. Phys. Chem.* **1996**, *100*, 7526−7532.
(33) Farnum, B. H.; Jou, J. J.; Meyer, G. J. *Proc. Natl. Acad. Sci. U. S. A.* **2012**, *109*, 15628−15633.
(34) Yonemoto, E. H.; Riley, R. L.; Kim, Y. Il; Atherton, S. J.; Schmehl, R. H.; Mallouk, T. E. *J. Am. Chem. Soc.* **1992**, *114*, 8081−8087.
(35) Cooley, L. F.; Larson, S. L.; Elliott, C. M.; Kelley, D. F. *J. Phys. Chem.* **1991**, *95*, 10694−10700.
(36) Roest, M. R.; Verhoeven, J. W.; Schuddeboom, W.; Warman, J. M.; Lawson, J. M.; Paddon-Row, M. N. *J. Am. Chem. Soc.* **1996**, *118*, 1762−1768.
(37) Weinhold, F.; Landis, C. *Valency and Bonding*; Cambridge University Press: Cambridge, 2005.
(38) Hoertz, P. G.; Staniszewski, A.; Marton, A.; Higgins, G. T.; Incarvito, C. D.; Rheingold, A. L.; Meyer, G. J. *J. Am. Chem. Soc.* **2006**, *132*, 8234−8245.
(39) Crosby, G. A.; Demas, J. N. *J. Phys. Chem.* **1971**, *75*, 991−1024.
(40) Argazzi, R.; Bignozzi, C. A.; Heimer, T. A.; Castellano, F. N.; Meyer, G. J. *Inorg. Chem.* **1994**, *33*, 5741−5749.
(41) Ruthkosky, M.; Castellano, F. N.; Meyer, G. J. *Inorg. Chem.* **1996**, *35*, 6406−6412.
(42) Manov, G. G.; Bates, R. G.; Hamer, W. J.; Acree, S. F. *J. Am. Chem. Soc.* **1943**, *65*, 1765−1767.
(43) *Gaussian 09*, Revision D.01. Frisch, M. J.; Trucks, G. W.; Schlegel, H. B.; Scuseria, G. E.; Robb, M. A.; Cheeseman, J. R.; Scalmani, G.; Barone, V.; Mennucci, B.; Petersson, G. A.; Nakatsuji, H.; Caricato, M.; Li, X.; Hratchian, H. P.; Izmaylov, A. F.; Bloino, J.; Zheng, G.; Sonnenberg, J. L.; Hada, M.; Ehara, M.; Toyota, K.; Fukuda, R.; Hasegawa, J.; Ishida, M.; Nakajima, T.; Honda, Y.; Kitao, O.; Nakai, H.; Vreven, T.; Montgomery, J. A., Jr.; Peralta, J. E.; Ogliaro, F.; Bearpark, M.; Heyd, J. J.; Brothers, E.; Kudin, K. N.; Staroverov, V. N.; Kobayashi, R.; Normand, J.; Raghavachari, K.; Rendell, A.; Burant, J. C.; Iyengar, S. S.; Tomasi, J.; Cossi, M.; Rega, N.; Millam, J. M.; Klene, M.; Knox, J. E.; Cross, J. B.; Bakken, V.; Adamo, C.; Jaramillo, J.; Gomperts, R.; Stratmann, R. E.; Yazyev, O.; Austin, A. J.; Cammi, R.; Pomelli, C.; Ochterski, J. W.; Martin, R. L.; Morokuma, K.; Zakrzewski, V. G.; Voth, G. A.; Salvador, P.; Dannenberg, J. J.; Dapprich, S.; Daniels, A. D.; Farkas, Ö.; Foresman, J. B.; Ortiz, J. V.; Cioslowski, J.; Fox, D. J. Gaussian, Inc.: Wallingford, CT, 2009.
(44) Lee, C.; Yang, W.; Parr, R. G. *Phys. Rev. B: Condens. Matter Mater. Phys.* **1988**, *37*, 785−789.
(45) Vosko, S. H.; Wilk, L.; Nusair, M. *Can. J. Phys.* **1980**, *58*, 1200−1211.
(46) Becke, A. D. *J. Chem. Phys.* **1993**, *98*, 5648−5652.
(47) Stephens, P. J.; Devlin, F. J.; Chabalowski, C. F.; Frisch, M. J. *J. Phys. Chem.* **1994**, *98*, 11623−11627.
(48) McLean, A. D.; Chandler, G. S. *J. Chem. Phys.* **1980**, *72*, 5639−5648.
(49) Hay, P. J.; Wadt, W. R. *J. Chem. Phys.* **1985**, *82*, 299−310.
(50) Hay, P. J.; Wadt, W. R. *J. Chem. Phys.* **1985**, *82*, 270−283.
(51) Wadt, W. R.; Hay, P. J. *J. Chem. Phys.* **1985**, *82*, 284−298.
(52) Ehlers, A. W.; Böhme, M.; Dapprich, S.; Gobbi, A.; Höllwarth, A.; Jonas, V.; Köhler, K. F.; Stegmann, R.; Veldkamp, A.; Frenking, G. *Chem. Phys. Lett.* **1993**, *208*, 111−114.
(53) Krishnan, R.; Binkley, J. S.; Seeger, R.; Pople, J. A. *J. Chem. Phys.* **1980**, *72*, 650−654.
(54) Feller, D. *J. Comput. Chem.* **1996**, *17*, 1571−1586.
(55) Schuchardt, K. L.; Didier, B. T.; Elsethagen, T.; Sun, L.; Gurumoorthi, V.; Chase, J.; Li, J.; Windus, T. L. *J. Chem. Inf. Model.* **2007**, *47*, 1045−1052.
(56) Glendening, E. D.; Reed, A. E.; Carpenter, J. E.; Weinhold, F. *NBO*, Version 3.1.
(57) Weinhold, F.; Carpenter, J. E. In *The Structure of Small Molecules and Ions*; Naaman, R., Vager, Z., Eds.; Springer US: Boston, MA, 1988; pp 227−236.
(58) Reed, A. E.; Weinstock, R. B.; Weinhold, F. *J. Chem. Phys.* **1985**, *83*, 735−746.

DOI: 10.1021/jacs.6b11337
J. Am. Chem. Soc. 2016, 138, 16815−16826

(59) Foster, J. P.; Weinhold, F. *J. Am. Chem. Soc.* **1980**, *102*, 7211−7218.
(60) Carpenter, J. E.; Weinhold, F. *J. Mol. Struct.: THEOCHEM* **1988**, *169*, 41−62.
(61) Reed, A. E.; Curtiss, L. A.; Weinhold, F. *Chem. Rev.* **1988**, *88*, 899−926.
(62) Reed, A. E.; Weinhold, F. *J. Chem. Phys.* **1983**, *78*, 4066−4073.
(63) Reed, A. E.; Weinhold, F. *J. Chem. Phys.* **1985**, *83*, 1736−1740.

DOI: 10.1021/jacs.6b11337
J. Am. Chem. Soc. 2016, 138, 16815−16826